


Topological Hall-like magnetoresistance humps in anomalous Hall loops caused by planar Hall effect

 Chunjie Yan,¹ Zui Tao,¹ Zhenyu Gao,¹ Zishuang Li,¹ Xiao Xiao,¹ Haozhe Wang,¹ Lina Chen,^{2,*} and Ronghua Liu^{1,†}
¹*Jiangsu Provincial Key Laboratory for Nanotechnology, National Laboratory of Solid State Microstructures and School of Physics, Nanjing University, Nanjing 210093, China*
²*School of Science, Nanjing University of Posts and Telecommunications, Nanjing 210023, China*
 (Received 11 June 2023; revised 22 August 2023; accepted 25 August 2023; published 7 September 2023)

Achievement of various topological spin textures, such as magnetic skyrmion and chiral domain walls, in heavy-metal/ferromagnet (FM) multilayer films with interfacial Dzyaloshinskii-Moriya interaction have attracted enormous attention owing to their topological nature, emergent electromagnetic properties, and potential applications in spintronics. The topological Hall effect (THE), an indicator to distinguish spin textures with nontrivial topology from the trivial collinear magnetic configurations, is usually characterized by the dome-shaped peak in anomalous Hall resistivity (AHR) loops. However, several other magnetoresistance effects could also cause this aberrant hump in AHR curves. Here, we systematically study the AHR loops with these aberrant humps under the coercivity $\mu_0 H_c$ as a function of the orientation of the magnetic field to the film plane in several Pt/FM/Pt films. Combining the simulation model of AHR and planar Hall magnetoresistance (PHMR), we demonstrate that this THE-like hump originates from the PHMR of the in-plane magnetization component due to magnetization is not saturated below saturation field in the out-of-plane AHR loop measurements. Our results indicate that the origin of these dome-shaped anomalous in transport measurements is manifold and should be examined carefully.

 DOI: [10.1103/PhysRevB.108.094414](https://doi.org/10.1103/PhysRevB.108.094414)
I. INTRODUCTION

Magnetoresistance (MR) is a fundamental phenomenon that plays an essential role in understanding magnetism, electron transport, and various technological applications of spin materials [1–5]. Up to now, various MR effects have been discovered, including anisotropic magnetoresistance (AMR) [3,6,7], anomalous Hall magnetoresistance [8], spin Hall magnetoresistance (SMR) [9–11], and so on. Among these, AMR, discovered by William in ferromagnetic metals in 1857, is an important physical phenomenon used first in spintronics. AMR refers to the change of resistance, in which the resistance, including longitudinal and transversal, relies on the orientation of the magnetization direction relative to the current flow in ferromagnetic materials. The transverse component of AMR is also called the planar Hall effect (PHE) despite the origin of PHE being different from the normal Hall effect [12–14]. The conventional AMR and PHE of thin films with in-plane magnetization are described as

$$\rho_{xx} = \rho_{xx}^0 + \Delta\rho_{xx}^{\text{ip}} m_x^2, \quad (1)$$

$$\rho_{xy} = \Delta\rho_{xy}^{\text{ip}} m_x m_y. \quad (2)$$

ρ_{xx}^0 is the resistivity when in-plane magnetization is oriented perpendicular to the current flow defined by the x axis; $\Delta\rho_{xx}^{\text{ip}}$ and $\Delta\rho_{xy}^{\text{ip}}$ denote the maximum resistivity changes due to AMR and PHE, respectively. m_x and m_y are the components of

in-plane magnetization along the x - and y axis. Very recently, however, Oepen *et al.* found that the inelastic-scattering probability at film interfaces is the largest for the magnetization M normal to the film [15]. This will also cause an additional AMR term, so-called anisotropic interface magnetoresistance (AIMR), in which the film resistance changes with a rotating M in the plane perpendicular to the current direction [see Fig. 1(c)]. AIMR exhibits the $\cos^2 \beta$ dependence, where β is the angle between M and the film normal [15–17]. Therefore, the general dependence of resistivity on magnetization orientation is expressed by

$$\rho_{xx} = \rho_{xx}^0 + \Delta\rho_{xx}^{\text{ip}} m_x^2 + \Delta\rho_{xx}^{\text{op}} m_z^2. \quad (3)$$

$\Delta\rho_{xx}^{\text{op}}$ denotes the maximum resistivity change due to AIMR and m_z is the magnetization component along the normal direction of the film, presented by the z axis. However, there exist many works to refer $\Delta\rho_{xx}^{\text{op}}$ signature as a fingerprint of SMR without considering the AIMR effect, especially for thin films and heterostructures [18–20].

The anomalous Hall resistance (AHR) is another well-known fundamental and subtle phenomenon due to magnetic materials' anomalous Hall effect (AHE). There are intrinsic and extrinsic mechanisms for AHE [21]. The former is related to the Berry-phase curvatures and is, therefore, the topological nature of the Hall currents due to breaking some basic symmetries, such as the exchange coupling and the spin-orbit coupling breaking the time-reversal and the chiral symmetries, respectively. The latter is correlated to spin-dependent scattering due to disorder via the side-jump and skew-scattering mechanisms. Generally, the AHE

*chenlina@njupt.edu.cn

†rhliu@nju.edu.cn

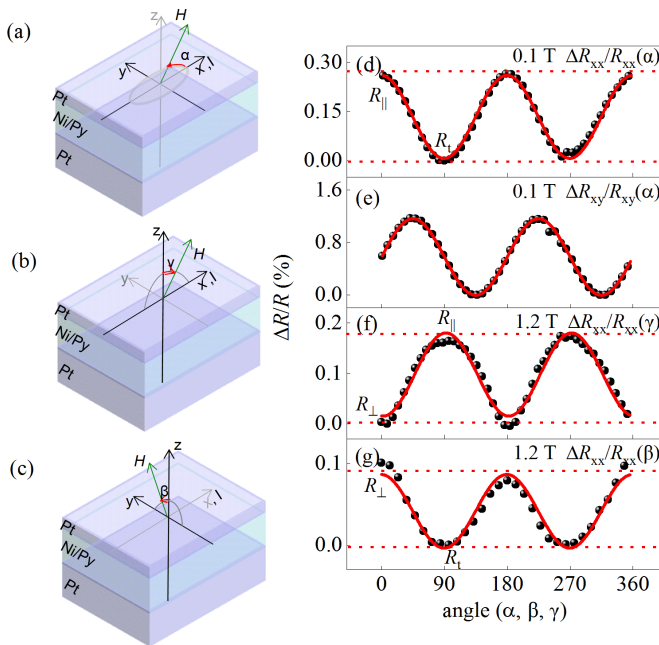


FIG. 1. (a)–(c) Schematic of longitudinal R_{xx} and transverse magnetoresistance R_{xy} measurements and definition of applied magnetic field angles α , β , and γ . α , β , and γ rotating in xy plane, yz plane, and xz plane, respectively. Applied current I is along x axis. (d)–(g) Symbols: Experimental $\Delta R_{xx}/R_{xx}$ and $\Delta R_{xy}/R_{xy}$ as function of angles α , γ , and β , defined in (a)–(c), measured at labeled magnetic fields in corresponding panel. Magnetization M parallels applied magnetic field $\mu_0 H$ in all these cases. Solid red curves are fitting curves. Horizontal dashed lines represent values of $R_{||}$, R_t , and R_{\perp} defined in main text.

signal is proportional to the saturation magnetization M_s in the ferromagnet, making the AHE one of the standard magnetometric techniques. In addition, spin-polarized carriers can obtain an extra Berry phase when passing through a certain real-space topological spin texture, resulting in lateral transport of the carriers [22]. As a result of this lateral transport, an additional Hall voltage characterized by an anomalous dome-shaped peak will emerge in AHR loops, which is proportional neither to the applied external magnetic field nor to the total magnetization, named the topological Hall effect (THE) [23–26]. Thus, THE, in turn, can be used to identify the topologically nontrivial spin textures, especially for the skyrmion phase or magnetic bubble domains with chiral domain walls in heavy-metal/ferromagnet (HM/FM) heterostructures with breaking of inversion symmetry [27–30]. However, as mentioned in AMR above, the observed additional dome-shaped Hall resistance in AHR loops would be caused by various MR effects besides THE in various HM/FM systems [31–33].

In this work, we demonstrate that the THE-like anomalous peak signal in AHR loops is related to PHE rather than THE of nontrivial spin textures, usually claimed in ultrathin magnetic multilayers with hybrid HM/FM, after systematically investigating field-dependent AMR and AHE loops in Pt/FM/Pt (FM = Ni/Py, Co/Ni) samples with in-plane magnetization. As the field is lower than the saturation field $\mu_0 H_s$, the magnetization of the FM layer has an in-plane component,

which will contribute an additional planar Hall magnetoresistance (PHMR) signal to append to the AHR and generate a dome-shaped peak under the $\mu_0 H_c$ in AHR loops. To provide further confirmation, we performed both the macrospin model and micromagnetic simulations, which qualitatively reproduce these experimental observations.

II. FABRICATION AND MAGNETORESISTANCE CHARACTERISTICS OF SAMPLES

Thin films with the structure of Pt(4 nm)/Ni(t_{Ni})/Py(t_{Py})/Pt(1 nm) are deposited on Si/SiO₂ substrate using dc-magnetron sputtering at room temperature. The base pressure is less than 2×10^{-8} Torr, and the Ar operation pressure is 3×10^{-3} Torr. The dependence of the magnetization on the external magnetic fields of the films is measured using a vibrating sample magnetometer, as shown in Supplemental Material [34] (see also Refs. [35–37] therein). The longitudinal and transverse resistances are measured using the standard four-probe technique. As shown in Figs. 1(a)–1(c), the AMR and PHMR are measured with a rotating external magnetic field higher than the saturation field in three typical planes. The electrical current I is applied along the longitudinal direction (x axis) of the ribbon sample. Figures 1(d)–1(g) show that the MR value exhibits the following rule: $R_{||} > R_{\perp} > R_t$, which is identical to the well-known AMR in most ferromagnetic metals [15–17], where $R_{||}$, R_t , and R_{\perp} are the longitudinal ($M \parallel I$ with in-plane M), transverse ($M \perp I$ with in-plane M), and perpendicular ($M \perp I$ with out-of-plane M) resistances, respectively. This characteristic indicates that the MR of the studied Pt/Ni/Py samples is dominated by the AIMR. The PHMR $\Delta R_{xy}/R_{xy}(\alpha)$ exhibits a $\cos \alpha \sin \alpha$ dependence [Fig. 1(e)], consistent with the PHE [13,14].

III. RESULTS AND DISCUSSION

A. In-plane magnetic field dependence of magnetoresistance

First, the longitudinal resistance R_{xx} of the sample was measured by sweeping an in-plane magnetic field with different in-plane angles α , as defined in Fig. 2(a). Based on the AMR effect, the angular-dependent R_{xx} exhibits a cosine function with a period of 180°. Therefore, as shown in Fig. 2(d), R_{xx} has the maximum value at $\alpha = 0^\circ$ and 180° , the median value at $\alpha = 45^\circ$ and 135° , and the minimum value at $\alpha = 90^\circ$. The same experiments were repeated for the transverse resistance R_{xy} . Compared to the angular-dependent R_{xx} , the angular-dependent transverse resistance R_{xy} has a phase shift of 45°, as shown in Fig. 1(e). Therefore, Fig. 2(c) shows that R_{xy} has the maximum and minimum values at $\alpha = 45^\circ$ and 135° , respectively. Note that in these longitudinal and transverse resistances versus the in-plane $\mu_0 H$ loops, two sharp peaks or dips appear around $\mu_0 H_c = 0.5$ mT. Similar peaks and dips are also observed at $R_{xy}(H)$ loops with the out-of-plane field, as shown in Fig. 3(b). These peaks and dips are related to the combination of AMR and multidomain structure due to magnetization switching around $\mu_0 H_c$, which will be discussed in detail in the micromagnetic simulation below [38,39].

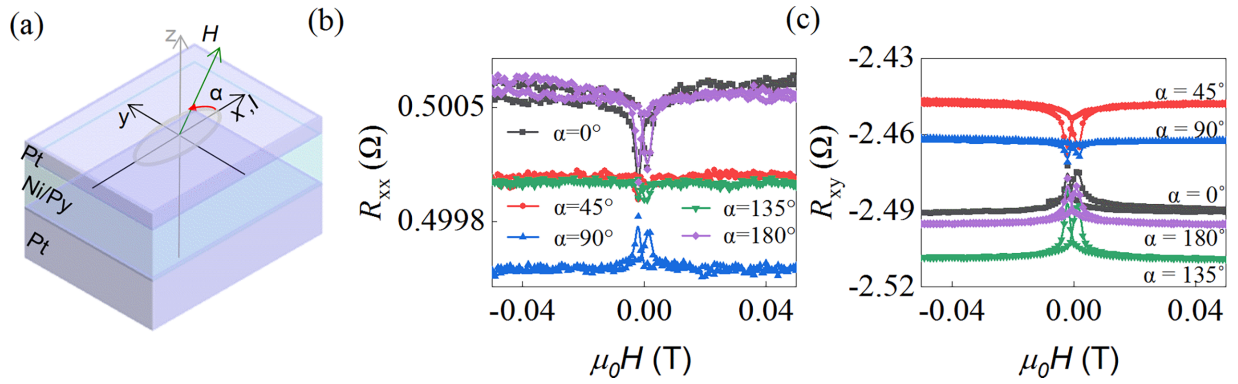


FIG. 2. (a) Schematic of field-dependent magnetoresistance measurement and definition of angle α between in-plane field μ_0H and current flow I . (b), (c) Longitudinal (b) and transverse (c) resistances under in-plane magnetic field with different angles α .

B. Out-of-plane magnetic field dependence of Hall resistance R_{xy}

To explore the possible interesting magnetic properties in these hybrid films, we further studied the transverse resistance R_{xy} signals as a function of the near out-of-plane external magnetic field μ_0H , as shown in Fig. 3(a). Figure 3(b) shows R_{xy} vs μ_0H loops with different orientations of μ_0H for Pt(4)Ni(2.0)Py(1.5)Pt(1) sample. The peak or dip

appearing near zero out-of-plane fields has the same origin as the observed peak or dips in the in-plane R_{xx} and R_{xy} . Besides, a pronounced hump appears in the fields lower than the coercive field μ_0H_c , significantly different from the conventional AHE [40]. These dome-shaped peaks in the AHR loops seem to correlate to various topological spin texture-induced THE [28,41,42], such as inverse Heusler thin-film Mn_2RhSn [28].

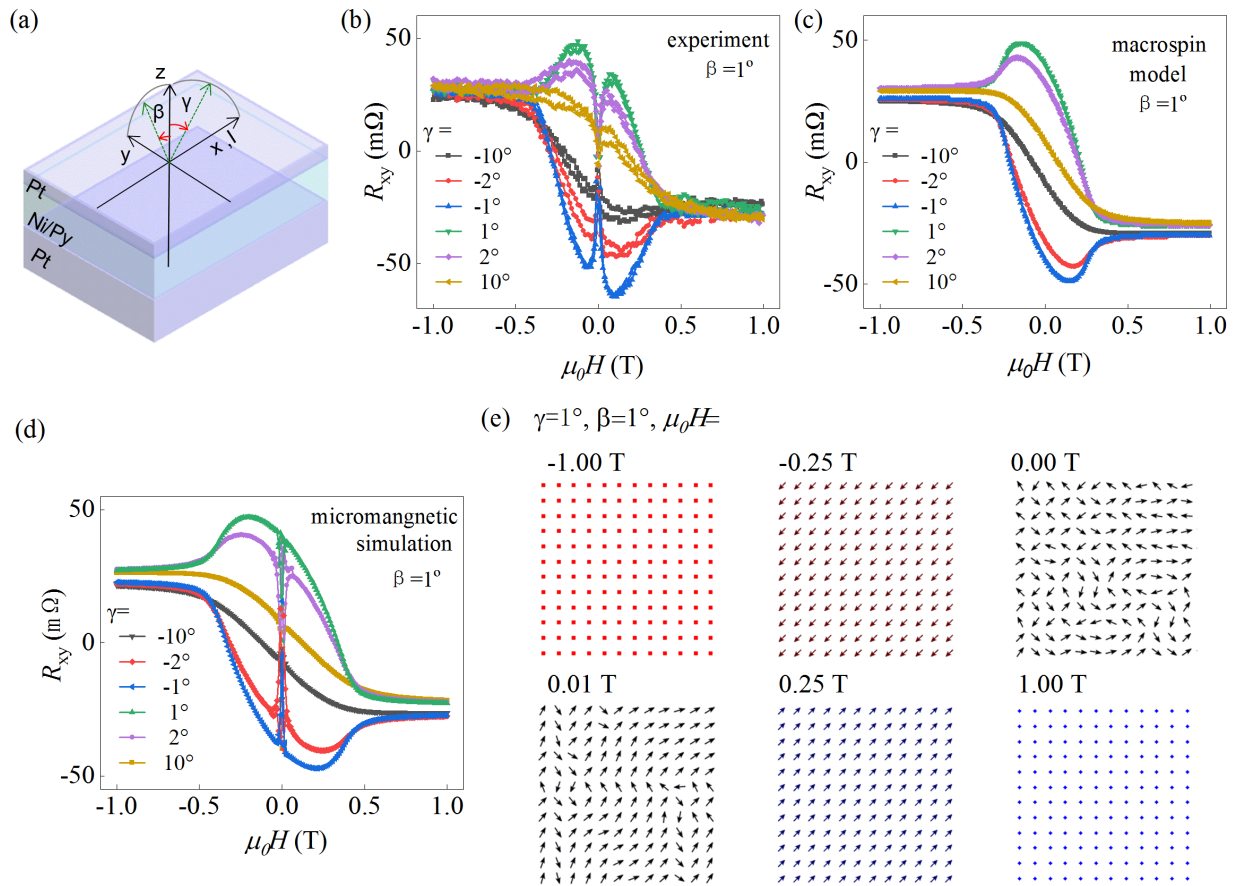


FIG. 3. (a) Schematic of transverse resistance R_{xy} measurements and definition of applied magnetic field angles β and γ , β and γ rotating in the yz plane and xz plane, respectively. (b)–(d) Experimental (b), macrospin model (c), and micromagnetic simulation (d) of R_{xy} vs μ_0H under near out-of-plane magnetic field with fixed $\beta = 1^\circ$ and several different γ , as labeled in panel, for Pt(4)Ni(2.0)Py(1.5)Pt(1) sample. (e) Magnetization snapshots obtained by micromagnetic simulation at labeled μ_0H with fixed $\beta = 1^\circ$ and $\gamma = 1^\circ$. Arrows represent in-plane component of M . Colors represent out-of-plane component of M .

However, THE cannot be the only origin of the observed humps in the transverse resistivity. The inhomogeneous magnetoelectric properties related to various MR effects discussed above can also cause these aberrant behaviors [31–33,43,44]. For example, Fu *et al.* reported that two types of aberrant humps observed near the magnetization-compensation temperature T_M in ferrimagnetic CoGd alloys are related to the spin-flop behavior and the composition inhomogeneity of CoGd alloys, respectively [31]. Kan *et al.* reported that typical humps of the AHE in SrRuO₃ would also be related to the inhomogeneous magnetoelectric properties of the film [33]. Chen *et al.* suggest that these THE-like hump features in synthetic antiferromagnetic and synthetic ferromagnetic multilayers result from the opposite coefficient of the AHE among different sublayers or interfaces due to the interfacial Pd-Co intermixing [32].

The observed dome-shaped peaks in our Pt/Ni/Py/Pt films are similar to them. However, after careful analysis of various MR effects mentioned above, we find that the PHE due to the in-plane component of magnetization M can explain the abnormal humps of the AHR near $\mu_0 H_c$. The reasons are as follows. When $\mu_0 H$ is below $\mu_0 H_c$, M has an in-plane component, contributing an additional PHMR signal to append to the AHR. As mentioned before, the PHE depends on the direction of the in-plane magnetization, which is determined by the in-plane orientation and magnitude of the applied out-of-plane field $\mu_0 H$. Therefore, we choose several deviation angles β (γ) of the external magnetic field from the z axis towards the y axis (x axis), defined in Fig. 3(a), as examples to illustrate the observed humps near $\mu_0 H_c$ arising from PHMR. Figure 3(b) shows several representative results of R_{xy} vs $\mu_0 H$ obtained at $\beta = 1^\circ$ and six selected angles: $\gamma = -10^\circ, -2^\circ, -1^\circ, 1^\circ, 2^\circ$, and 10° . According to the symmetry of the PHE [as shown in Fig. 1(e) and Fig. 2(c)], a maximum resistance of the PHE is expected for the magnetization in-plane angle $\alpha = 45^\circ$ corresponding to $\beta = \gamma = 1^\circ$, while a minimum is at $\alpha = 135^\circ$ ($\beta = 1^\circ$ and $\gamma = -1^\circ$). These maxima and minima will result in the abnormal dome and valley in R_{xy} vs $\mu_0 H$ loops in Fig. 3(b).

C. Numerical results of the macrospin model and micromagnetic simulations

To further confirm the deduction, we perform the numerical calculation of R_{xy} vs $\mu_0 H$ loop using a general analytic formula including the ordinary Hall effect (OHE), AHE, and PHE:

$$\rho_{xy} = \rho_0 H_z + \Delta\rho_{\text{AHE}} m_z + \Delta\rho_{xy}^{\text{ip}} m_x m_y, \quad (4)$$

where ρ_0 , $\Delta\rho_{\text{AHE}}$, $\Delta\rho_{xy}^{\text{ip}}$ are the OHE, AHE, and PHE coefficients, respectively. m_x , m_y , and m_z are the normalized magnetization components $\frac{M}{M_s}$ along the x -, y -, and z axis, respectively. We can obtain the orientation of magnetization under different magnetic fields by minimizing the system's total energy, and the data are shown in Supplemental Material, Note 2 [34]. Figure 3(c) shows the calculated results of the macrospin model at the selected angles β and γ of the external field, reproducing the experimentally observed anomalous hump, as shown in Fig. 3(b). To better illustrate the evolution process of the magnetic texture with the tilted

TABLE I. Summary of fitting parameters for angular-dependent MR experiments and numerical calculation humps in R_{xy} vs $\mu_0 H$.

$t_{\text{Ni}}/t_{\text{Py}}$ (nm)	$\frac{\Delta R_{xy}}{R_{xy}}$ (PHE fitting)	$\Delta R_{xy}^{\text{ip}}$ (calculation)
2.0/1.5	0.012 ± 0.001	0.013 ± 0.001
2.5/1.5	0.023 ± 0.001	0.025 ± 0.002
3.0/1.5	0.011 ± 0.001	0.007 ± 0.001
2.5/1.0	0.019 ± 0.002	0.012 ± 0.002
0.0/4.0	0.020 ± 0.001	0.027 ± 0.002

magnetic field, we further performed the micromagnetic simulations of the M vector as a function of $\mu_0 H$ with $\beta = 1^\circ$ and $\gamma = -10^\circ, -2^\circ, -1^\circ, 1^\circ, 2^\circ$, and 10° by using OOMMF code with material parameters $M = 3.0 \times 10^5$ A/m. The simulated volume is a square of $1 \mu\text{m} \times 1 \mu\text{m}$ with a thickness of 3.5 nm, which is divided into $5 \times 5 \times 3.5 \text{ nm}^3$ cells. To get the MR hysteresis loops, we first integrate all individual M vectors obtained by OOMMF simulation into an average magnetization vector \mathbf{m} (m_x, m_y, m_z), then use the MR-effect equation [Eq. (4)] to convert the simulated M vs $\mu_0 H$ loops to R_{xy} vs $\mu_0 H$ loops. Figure 3(d) shows the representative simulation results of R_{xy} vs $\mu_0 H$ loops at the selected angles β and γ of the external field, consistent with the macrospin model and well reproducing the experimentally observed anomalous hump at 0.25 mT and sharp peaks or dips near zero fields. Figure 3(e) shows the magnetization snapshots obtained at the six representative $\mu_0 H$ with a fixed $\beta = 1^\circ$ and $\gamma = 1^\circ$. As discussed above, the \mathbf{m} has a significant in-plane magnetization component along the in-plane field component for the fields lower than the coercive field $\mu_0 H_c$ [Fig. 3(e)], which generates a pronounced hump due to the AMR effect. The multidomain structure appears at the low fields due to the competition among the exchange energy, Zeeman energy, and demagnetization energy, which gives rise to the peaks or dips in R_{xy} vs $\mu_0 H$ curves due to the AMR effect.

D. Experimental results and numerical results for other FM multilayer systems

To see if this anomalous behavior is universal for other similar multilayer systems, we repeat the measurements and numerical calculations of R_{xy} vs $\mu_0 H$ loops for a series of Pt(4)/Ni(t_{Ni})/Py(t_{Py})/Pt(1) samples with different FM thicknesses. First, we measure the PHMR as a function of the in-plane field angle α at $\mu_0 H = 0.1$ T, higher than the saturation field of these materials, as shown in Fig. 4(a). R_{xy} of Pt(4 nm)/Ni/Py/Pt(1 nm) systems with different Ni or Py thicknesses can be well fitted by a $\cos \alpha \sin \alpha$ function, consistent with the PHE. The PHE parameters $\frac{\Delta R_{xy}}{R_{xy}}$ are fitted and summarized in Table I. Figure 4(b) shows R_{xy} vs $\mu_0 H$ results with $\beta = \gamma = 1^\circ$. All samples show pronounced humps near the field lower than the coercive field H_c . As we know, the AHE of the FM is known to be proportional to the saturation magnetization M_s , i.e., $\rho_{xy}^{\text{AH}} = R_s M_s$, where R_s is the anomalous Hall coefficient. From the hysteresis loops characterized by vibrating sample magnetometer (VSM), we can deduce the out-of-plane magnetic field dependence of R_{xy}^{AH} only arise from AHE [shown in Fig. 4(b), red square]. The residual ΔR_{xy}

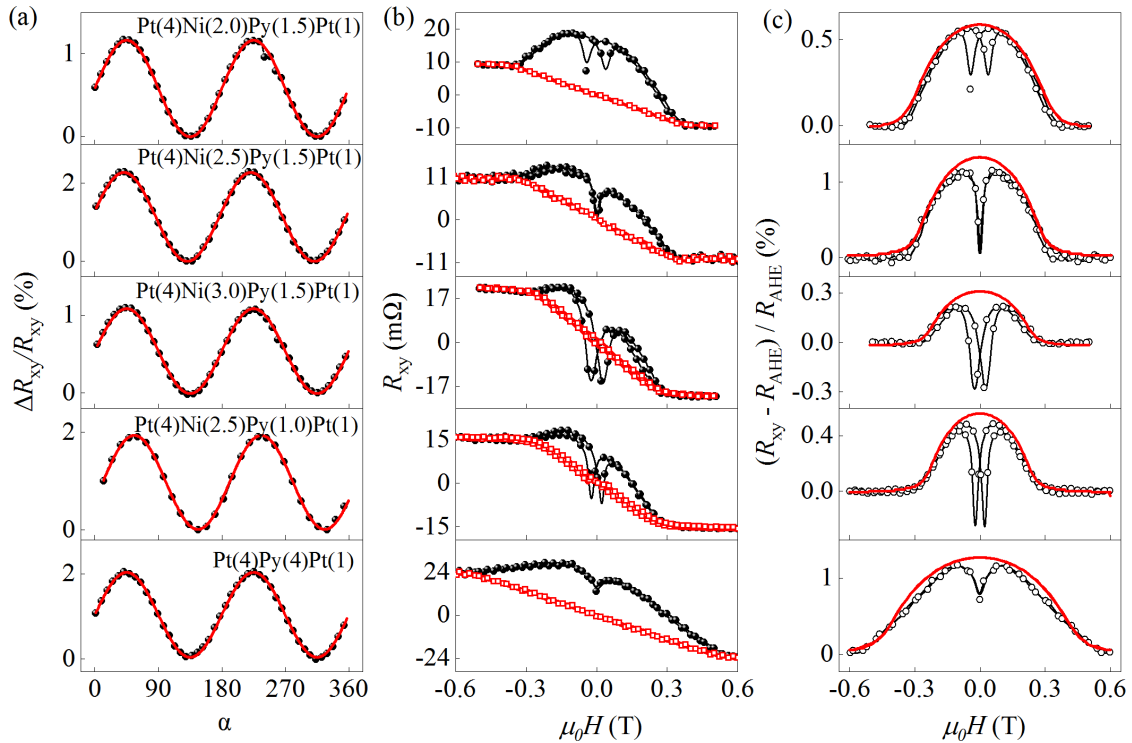


FIG. 4. (a) Symbols: Experimental $\frac{\Delta R_{xy}}{R_{xy}}$ as function of in-plane field angle α for Pt/(Ni/Py or Py)/Pt samples. Solid red lines: Fitting curves using PHE model. (b) Experimental transverse resistance R_{xy} vs $\mu_0 H$ loops (solid black circle) under near out-of-plane magnetic field $\mu_0 H$ with $\gamma = 1^\circ$ and $\beta = 1^\circ$ and normalized AHR R_{AHE} vs $\mu_0 H$ calculated from M vs $\mu_0 H$ loops (red square) measured by VSM. (c) Experimental R_{xy} after being subtracted from R_{AHE} background as function of $\mu_0 H$ with $\gamma = 1^\circ$ and $\beta = 1^\circ$ (black circle) and simulation curves (red line).

with a hump below H_c after subtracting R_{xy}^{AH} from the total R_{xy} is shown in Fig. 4(c) (symbol). These residual ΔR_{xy} curves can be well fitted by using PHMR $\sim \Delta R_{xy}^{ip} m_x m_y$ with the parameter ΔR_{xy}^{ip} in Table I. The solid red lines are the fitting results in Fig. 4(c).

The corresponding MR ratios $\Delta R_{xy}/R_{xy}$ extracted from in-plane PHE and the parameter ΔR_{xy}^{ip} used in out-of-plane PHMR simulation are summarized in Table I. As one can see, the parameters ΔR_{xy}^{ip} used in the simulation in Fig. 4(c) well agree with the planar Hall coefficient obtained by fitting the PHE as a function of the in-plane field angle, as shown in Fig. 4(a). Moreover, Pt(5)/[Co(0.2)/Ni(0.6)]₁₀/Pt(1), as shown in Supplemental Material, Note 3 [34], and the previously reported Pt/yttrium iron garnet [45] with in-plane anisotropy also exhibit a similar hump in R_{xy} vs $\mu_0 H$ loops, indicating that it is a universal phenomenon arising from the PHE for many magnetic thin-film systems without any topological spin textures.

IV. CONCLUSIONS

In summary, the field- and angular-dependent MR in Pt/Ni/Py/Pt and Pt/[Co/Ni]_n/Pt samples were investigated for both in-plane and out-of-plane orientations. In-plane angular-

dependent R_{xy} and R_{xx} curves show that these hybrid systems exhibit a strong AIMR besides the conventional AMR/PHMR. Out-of-plane R_{xy} vs $\mu_0 H$ exhibits aberrant humps, like the THE-induced Hall resistance, which strongly depends on the deviation angle of the field. After performing systematic measurements and careful analysis, we demonstrate that these THE-like humps observed in R_{xy} vs $\mu_0 H$ loops are caused by the PHE of the in-plane magnetization component due to magnetization that is not saturated below the saturation field, which is a universal effect existing in many magnetic systems. Therefore, our findings warn that more attention should be paid to abnormal surprises in MR measurements and avoid excessive attribution to the topological Hall effect.

ACKNOWLEDGMENTS

This work was supported by the National Natural Science Foundation of China (NNSFC) (Grants No. 12074178 and No. 12004171), the Applied Basic Research Programs of Science and Technology Commission Foundation of Jiangsu Province (Grant No. BK20200309), and the Open Research Fund of Jiangsu Provincial Key Laboratory for Nanotechnology, the Scientific Foundation of Nanjing University of Posts and Telecommunications (NUPTSF) (Grant No. NY220164).

[1] T. Q. Hung, J.-R. Jeong, D.-Y. Kim, N. Huu Duc, and C. G. Kim, Hybrid planar Hall-magnetoresistance sensor based on tilted cross-junction, *J. Phys. D: Appl. Phys.* **42**, 055007 (2009).

[2] G. Liu, X.-g. Wang, Z. Z. Luan, L. F. Zhou, S. Y. Xia, B. Yang, Y. Z. Tian, G.-h. Guo, J. Du, and D. Wu, Magnonic Unidirectional Spin Hall Magnetoresistance in a

- Heavy-Metal-Ferromagnetic-Insulator Bilayer, *Phys. Rev. Lett.* **127**, 207206 (2021).
- [3] F. L. Zeng, Z. Y. Ren, Y. Li, J. Y. Zeng, M. W. Jia, J. Miao, A. Hoffmann, W. Zhang, Y. Z. Wu, and Z. Yuan, Intrinsic Mechanism for Anisotropic Magnetoresistance and Experimental Confirmation in $\text{Co}_x\text{Fe}_{1-x}$ Single-Crystal Films, *Phys. Rev. Lett.* **125**, 097201 (2020).
- [4] H. Nakayama, Y. Kanno, H. An, T. Tashiro, S. Haku, A. Nomura, and K. Ando, Rashba-Edelstein Magnetoresistance in Metallic Heterostructures, *Phys. Rev. Lett.* **117**, 116602 (2016).
- [5] Y. Wang, P. A. Lee, D. M. Silevitch, F. Gomez, S. E. Cooper, Y. Ren, J.-Q. Yan, D. Mandrus, T. F. Rosenbaum, and Y. Feng, Antisymmetric linear magnetoresistance and the planar Hall effect, *Nat. Commun.* **11**, 216 (2020).
- [6] L. K. Zou, Y. Zhang, L. Gu, J. W. Cai, and L. Sun, Tunable angular-dependent magnetoresistance correlations in magnetic films and their implications for spin Hall magnetoresistance analysis, *Phys. Rev. B* **93**, 075309 (2016).
- [7] S. S.-L. Zhang and S. Zhang, Angular dependence of anisotropic magnetoresistance in magnetic systems, *J. Appl. Phys.* **115**, 17C703 (2014).
- [8] Y. Yang, Z. Luo, H. Wu, Y. Xu, R.-W. Li, S. J. Pennycook, S. Zhang, and Y. Wu, Anomalous Hall magnetoresistance in a ferromagnet, *Nat. Commun.* **9**, 2255 (2018).
- [9] M. Althammer, S. Meyer, H. Nakayama, M. Schreier, S. Altmannshofer, M. Weiler, H. Huebl, S. Geprägs, M. Opel, R. Gross, D. Meier, C. Klewe, T. Kuschel, J.-M. Schmalhorst, G. Reiss, L. Shen, A. Gupta, Y.-T. Chen, G. E. W. Bauer, E. Saitoh, and S. T. B. Goennenwein, Quantitative study of the spin Hall magnetoresistance in ferromagnetic insulator/normal metal hybrids, *Phys. Rev. B* **87**, 224401 (2013).
- [10] B. F. Miao, S. Y. Huang, D. Qu, and C. L. Chien, Inverse Spin Hall Effect in a Ferromagnetic Metal, *Phys. Rev. Lett.* **111**, 066602 (2013).
- [11] H. Nakayama, M. Althammer, Y.-T. Chen, K. Uchida, Y. Kajiwara, D. Kikuchi, T. Ohtani, S. Geprägs, M. Opel, S. Takahashi, R. Gross, G. E. W. Bauer, S. T. B. Goennenwein, and E. Saitoh, Spin Hall Magnetoresistance Induced by a Nonequilibrium Proximity Effect, *Phys. Rev. Lett.* **110**, 206601 (2013).
- [12] É. M. Épshtein, Planar Hall effect in ferromagnets, *Phys. Solid State* **44**, 1327 (2002).
- [13] Z. Q. Lu, G. Pan, and W. Y. Lai, Planar Hall effect in NiFe/NiMn bilayers, *J. Appl. Phys.* **90**, 1414 (2001).
- [14] N. Naftalis, A. Kaplan, M. Schultz, C. A. F. Vaz, J. A. Moyer, C. H. Ahn, and L. Klein, Field-dependent anisotropic magnetoresistance and planar Hall effect in epitaxial magnetite thin films, *Phys. Rev. B* **84**, 094441 (2011).
- [15] A. Kobs, S. Heße, W. Kreuzpaintner, G. Winkler, D. Lott, P. Weinberger, A. Schreyer, and H. P. Oepen, Anisotropic Interface Magnetoresistance in Pt/Co/Pt Sandwiches, *Phys. Rev. Lett.* **106**, 217207 (2011).
- [16] A. Kobs and H. P. Oepen, Disentangling interface and bulk contributions to the anisotropic magnetoresistance in Pt/Co/Pt sandwiches, *Phys. Rev. B* **93**, 014426 (2016).
- [17] A. Philipp-Kobs, A. Farhadi, L. Matheis, D. Lott, A. Chuvilin, and H. P. Oepen, Impact of Symmetry on Anisotropic Magnetoresistance in Textured Ferromagnetic Thin Films, *Phys. Rev. Lett.* **123**, 137201 (2019).
- [18] S.-Y. Huang, H.-L. Li, C.-Wei Chong, Y.-Y. Chang, M.-K. Lee, and J.-C.-A. Huang, Interface-induced spin Hall magnetoresistance enhancement in Pt-based tri-layer structure, *Sci. Rep.* **8**, 108 (2018).
- [19] Y. Hui, H. Jiang, F. Xie, W. Lin, C. Dong, K. Dong, Q. He, and X. Miao, Maximizing spin Hall magnetoresistance in heavy metal/crystalline metallic ferromagnet multilayers with opposite spin Hall angles, *Nanoscale* **15**, 820 (2023).
- [20] S. Zhang, S. Xia, Q. Li, B. Yang, J. Li, Q. Cao, D. Wang, R. Liu, and Y. Du, Identification of spin-dependent thermoelectric effects in metamagnetic FeRh/heavy-metal bilayers, *Appl. Phys. Lett.* **118**, 142401 (2021).
- [21] N. Nagaosa, J. Sinova, S. Onoda, A. H. MacDonald, and N. P. Ong, Anomalous Hall effect, *Rev. Mod. Phys.* **82**, 1539 (2010).
- [22] N. Nagaosa and Y. Tokura, Topological properties and dynamics of magnetic skyrmions, *Nat. Nanotechnol.* **8**, 899 (2013).
- [23] M. Raju, A. Yagil, A. Soumyanarayanan, A. K. C. Tan, A. Almoalem, F. Ma, O. M. Auslaender, and C. Panagopoulos, The evolution of skyrmions in Ir/Fe/Co/Pt multilayers and their topological Hall signature, *Nat. Commun.* **10**, 696 (2019).
- [24] Z. S. Lim, C. Li, Z. Huang, X. Chi, J. Zhou, S. Zeng, G. J. Omar, Y. P. Feng, A. Rusydi, S. J. Pennycook, T. Venkatesan, and A. Ariando, Emergent topological Hall effect at a charge-transfer interface, *Small* **16**, 2004683 (2020).
- [25] S. Xia, S. Zhang, Z. Luan, L. Zhou, J. Liang, G. Liu, B. Yang, H. Yang, R. Liu, and D. Wu, Interfacial Dzyaloshinskii-Moriya interaction between ferromagnetic insulator and heavy metal, *Appl. Phys. Lett.* **116**, 052404 (2020).
- [26] A. Laha, R. Singha, S. Mardanya, B. Singh, A. Agarwal, P. Mandal, and Z. Hossain, Topological Hall effect in the antiferromagnetic Dirac semimetal EuAgAs, *Phys. Rev. B* **103**, L241112 (2021).
- [27] K. K. Meng, X. P. Zhao, P. F. Liu, Q. Liu, Y. Wu, Z. P. Li, J. K. Chen, J. Miao, X. G. Xu, J. H. Zhao, and Y. Jiang, Robust emergence of a topological Hall effect in MnGa/heavy metal bilayers, *Phys. Rev. B* **97**, 060407(R) (2018).
- [28] P. K. Sivakumar, B. Göbel, E. Lesne, A. Markou, J. Gidugu, J. M. Taylor, H. Deniz, J. Jena, C. Felser, I. Mertig, and S. S. P. Parkin, Topological Hall signatures of two chiral spin textures hosted in a single tetragonal inverse Heusler thin film, *ACS Nano* **14**, 13463 (2020).
- [29] X. Liu, Q. Feng, D. Zhang, Y. Deng, S. Dong, E. Zhang, W. Li, Q. Lu, K. Chang, and K. Wan, Topological spin textures in a non-collinear antiferromagnet system, *Adv. Mater.* **35**, 2211634 (2023).
- [30] S. Zhang, S. Xia, Q. Cao, D. Wang, R. Liu, and Y. Du, Observation of topological Hall effect in antiferromagnetic FeRh film, *Appl. Phys. Lett.* **115**, 022404 (2019).
- [31] T. Fu, S. Li, X. Feng, Y. Cui, J. Yao, B. Wang, J. Cao, Z. Shi, D. Xue, and X. Fan, Complex anomalous Hall effect of CoGd alloy near the magnetization compensation temperature, *Phys. Rev. B* **103**, 064432 (2021).
- [32] R. Y. Chen, R. Q. Zhang, Y. J. Zhou, H. Bai, F. Pan, and C. Song, Magnetic field direction dependence of topological Hall effect like features in synthetic ferromagnetic and antiferromagnetic multilayers, *Appl. Phys. Lett.* **116**, 242403 (2020).
- [33] D. Kan, T. Moriyama, K. Kobayashi, and Y. Shimakawa, Alternative to the topological interpretation of the transverse resistivity anomalies in SrRuO₃, *Phys. Rev. B* **98**, 180408(R) (2018).
- [34] See Supplemental Material at <http://link.aps.org/supplemental/10.1103/PhysRevB.108.094414> for the calculated equilib-

- rium orientations of magnetization and the similar hump in Pt(5)[Co(0.2)Ni(0.6)]₁₀Pt(1).
- [35] A. K. Dhiman, T. Dohi, W. Dobrogowski, Z. Kurant, I. Sveklo, S. Fukami, H. Ohno, and A. Maziewski, Magnetization processes and magnetic domain structures in Ta/CoFeB/MgO stacks, *J. Magn. Magn. Mater.* **529**, 167699 (2021).
- [36] M. Kisielewski, A. Maziewski, M. Tekielak, J. Ferré, S. Lemerle, V. Mathet, and C. Chappert, Magnetic anisotropy and magnetization reversal processes in Pt/Co/Pt films, *J. Magn. Magn. Mater.* **260**, 231 (2003).
- [37] C. Yan, L. Chen, K. Zhou, L. Yang, Q. Fu, W. Wang, W.-C. Yue, L. Liang, Z. Tao, J. Du, Y.-L. Wang, and R. Liu, Thickness-dependent magnetic properties in Pt/[Co/Ni]_n multilayers with perpendicular magnetic anisotropy, *Chin. Phys. B* **32**, 017503 (2022).
- [38] L. Chen, X. Zhan, K. Zhou, W. Wang, L. Liang, Z. Gao, Y. W. Du, and R. H. Liu, Spin-Orbit-Torque Efficiency and Current-Driven Coherent Magnetic Dynamics in a Pt/Ni/Py Trilayer-Based Spin Hall Nano-Oscillator, *Phys. Rev. Appl.* **17**, 064041 (2022).
- [39] L. Chen, W. Wang, X. Zhan, K. Zhou, Z. Gao, L. Liang, T. Zhou, Y. Du, and R. Liu, Spatial coexistence of multiple modes in a nano-gap spin Hall nano-oscillator with the extended Pt Ni Fe trilayers, *Phys. Rev. B* **105**, 104413 (2022).
- [40] P. Zhang, K. Xie, W. Lin, D. Wu, and H. Sang, Anomalous Hall Effect in Co/Ni multilayers with perpendicular magnetic anisotropy, *Appl. Phys. Lett.* **104**, 082404 (2014).
- [41] A. J. Lee, A. S. Ahmed, J. Flores, S. Guo, B. Wang, N. Bagués, D. W. McComb, and F. Yang, Probing the Source of the Interfacial Dzyaloshinskii-Moriya Interaction Responsible for the Topological Hall Effect in Metal/Tm₃Fe₅O₁₂ Systems, *Phys. Rev. Lett.* **124**, 107201 (2020).
- [42] A. S. Ahmed, A. J. Lee, N. Bagués, B. A. McCullian, A. M. A. Thabt, A. Perrine, P.-K. Wu, J. R. Rowland, M. Randeria, P. C. Hammel, D. W. McComb, and F. Yang, Spin-Hall topological hall effect in highly tunable Pt/ferrimagnetic-insulator bilayers, *Nano Lett.* **19**, 5683 (2019).
- [43] Y. Wang, C. Li, H. Zhou, J. Wang, G. Chai, and C. Jiang, Unusual anomalous Hall effect in the ferrimagnetic GdFeCo alloy, *Appl. Phys. Lett.* **118**, 071902 (2021).
- [44] A. Gerber, Interpretation of experimental evidence of the topological Hall effect, *Phys. Rev. B* **98**, 214440 (2018).
- [45] N. Vlietstra, J. Shan, V. Castel, B. J. van Wees, and J. Ben Youssef, Spin-Hall magnetoresistance in platinum on yttrium iron garnet: Dependence on platinum thickness and in-plane/out-of-plane magnetization, *Phys. Rev. B* **87**, 184421 (2013).